Available online at www.sciencedirect.com
SCIENCE DIRECT®
International Journal of Heat and Mass Transfer 47 (2004) 2913–2926
International Journal of HEAT and MASS TRANSFER
www.elsevier.com/locate/ijhmt

Double-diffusive natural convection in parallelogrammic enclosures

V.A.F. Costa *

Departamento de Engenharia Mecânica, Universidade de Aveiro, Campus Universitário de Santiago, 3810-193 Aveiro, Portugal

Received 11 February 2002; received in revised form 19 March 2004

Abstract

Double-diffusive natural convection in parallelogrammic enclosures filled with moist air is studied numerically. This geometry presents high potential for heat and/or mass transfer, since it can act as a heat and/or mass transfer promoter or as a heat and/or mass transfer inhibitor, being referred to as a heat and/or mass transfer diode. Work is concentrated on the physical modeling and on the analysis of a set of numerical results, obtained for some combinations of the dimensionless governing parameters, for two-dimensional parallelogrammic enclosures. The heat and mass transfer characteristics of the parallelogrammic enclosure are analyzed using the streamlines, heatlines and masslines. Its transfer performances are analyzed and it is explored the dependence of the global Nusselt and Sherwood numbers on the thermal Rayleigh number, aspect ratio and inclination angle, both for the situations of combined and opposite global heat and mass flows through the enclosure. Relevant information can be extracted from the presented results in what concerns the overall heat and/or mass transfer performance of the parallelogrammic enclosures, and how selected combinations of the governing parameters can lead to maximum or minimum overall transfer. The heat and/or mass transfer diode effect of this shape is also highlighted. Results clearly show the high potential of the parallelogrammic enclosures, which can be used alone or taken as the basic form to obtain, by assembly, most complete and even complex efficient heat and/or mass transfer systems.

1. Introduction

Double-diffusive natural convection in enclosures has received special attention in many recent works, concerning both enclosures filled with a fluid only [1–8] or enclosures filled with fluid-saturated porous media [9–18], just to mention a few of such works. To the best knowledge of the author, no attention has been paid to the double-diffusive natural convection in parallelogrammic enclosures. It is a geometry with important features and potential in what concerns heat and mass transfer performance, the parallelogrammic enclosure having different heat and mass transfer performance for different inclination angles and different aspect ratios. It can even present very different heat and/or mass transfer behavior for positive and for negative inclination angles, being referred to as a heat and/or mass transfer diode.

Natural convection in parallelogrammic enclosures has been previously studied [19–24], concerning both flow features and thermal performance. In the work reported in [19], results are presented for the flow structure and for the Nusselt number, this latter for some different combinations of Rayleigh number, Prandtl number, aspect ratio and inclination angle. Studies conducted in [21] deal with the transient natural convection in parallelogrammic enclosures, where analysis is made on the time evolution of the flow structure, vertical velocity, and global Nusselt number for different inclination angles and aspect ratios. For sufficiently long times, the steady-sate solution is obtained for each of the analyzed variables and combinations of parameters, and analysis is made of the global Nusselt number

* Tel.: +351-234-370-829; fax: +351-234-370-953.
E-mail address: v_costa@mec.ua.pt (V.A.F. Costa).

0017-9310/$ - see front matter © 2004 Elsevier Ltd. All rights reserved.
doi:10.1016/j.ijheatmasstransfer.2004.03.008

Nomenclature

C	concentration
D	mass diffusivity
g	gravitational acceleration
H	height
H	heatfunction
k	thermal conductivity
L	length
Le	Lewis number
m	mass
M	molar mass
M	massfunction
n	outward normal
N	buoyancy ratio
Nu	Nusselt number
p	pressure
Pr	Prandtl number
Ra	Rayleigh number
Sc	Schmidt number
Sh	Sherwood number
T	temperature
u, v	Cartesian velocity components
W	specific humidity, dry basis
x, y	Cartesian co-ordinates

Greek symbols

α	thermal diffusivity
β	volumetric expansion coefficient
θ	inclination angle
v	kinematic viscosity
ρ	density
ψ	streamfunction

Subscripts

C	referring concentration
H	higher value
L	lower value
p	referring pressure
T	referring temperature
*	dimensionless

dependence on some of the governing parameters. Work reported in [19,22] includes, additionally, the influence of the thermal conductivity of the separating walls of contiguous parallelogrammic enclosures assembled in a vertical stack, assuming that the conditions are the same in each enclosure in the assembly (vertical periodicity). Studies in [19,21] include the effect of the inclination angle and of the aspect ratio on the thermal performance of the enclosure. In what concerns thermal performance, results clearly show its strong dependence on the inclination angle and on the aspect ratio, the parallelogrammic enclosures having strong potential to be used as the basic structure that, by assembly, lead to high performance heat transfer elements to be used in many fields. It is a form that presents also a strong potential for a variable geometry structure, the inclination angle being changed by rotating the inclined walls of the enclosure, in order to achieve the desired (and considerably different) thermal performance at each time. In particular, the parallelogrammic enclosure presents special potential to act as a heat transfer inhibitor (thermal insulation) or to act as a heat transfer promoter (heat transfer enhancement), relative to the basic two-dimensional rectangular or square enclosures.

Many situations of practical interest deal with enclosures filled with a two-component mixture of an indifferent fluid and a pollutant whose mass transfer occurs, thus motivating the study of the double-diffusive natural convection problem in enclosures of parallelogrammic geometry. The governing dimensionless parameters are in number of 6, the presented results corresponding to only some particular combinations of such parameters. Additionally to the six governing parameters, the boundary conditions can be specified such that the global heat and mass flows are combined or opposite. Also the temperature and concentration buoyancy effects can be combined or opposite.

For parallelogrammic enclosures filled with moist air, the visualization of the occurring heat and mass transfer is analyzed in detail using the streamlines, heatlines and masslines [7,25]. Special emphasis is devoted to the analysis of the Nusselt and Sherwood numbers dependence on the dimensionless governing parameters for parallelogrammic enclosures filled with moist air. Questions related with multiple solutions or oscillatory solutions [10,13,15] are not analyzed, and combinations of the dimensionless governing parameters and boundary conditions leading to such solutions are intentionally avoided.

2. Physical and numerical modeling

2.1. Physical model

The domain under analysis is sketched in Fig. 1, where a parallelogrammic two-dimensional enclosure filled with a fluid containing a pollutant whose mass transfer occurs is under the influence of the gravity field. The walls of height H are always vertical walls, and the other walls of length L form an angle θ relative to the horizontal direction, being referred to as *inclined walls*. Some ratios H/L and angles θ are explored in order to

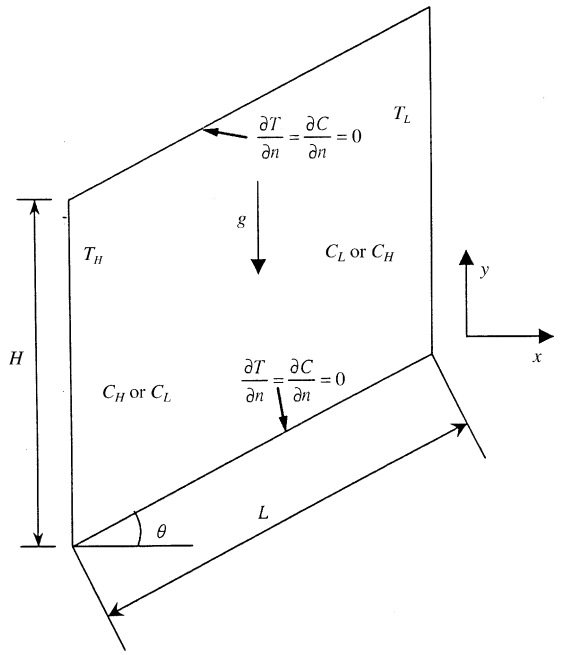

Fig. 1. Physical model and geometry.

analyze the structure of the resulting flow and the heat and mass transfer processes taking place.

The vertical walls are maintained at constant different levels of temperature and concentration, thus giving rise to a double-diffusive natural convection problem. The inclined walls are assumed to be impermeable and perfect thermal insulators.

2.2. Model assumptions

The indifferent fluid and the transported pollutant are assumed to be completely mixed. This mixture is the Newton–Fourier fluid that fills the cavity, which flows in laminar regime and does not experience any phase change. The mixture is taken as incompressible but expands or contracts under temperature and/or concentration changes.

The mixture density is assumed to be uniform over all the cavity, exception made to the buoyancy term, in which it is taken as a function of both the temperature and concentration levels through the Boussinesq approach. From $\rho = \rho(T, C)$, Thermodynamics teaches that $\beta_T = -(\partial\rho/\partial T)_{p,C}/\rho$ is the volumetric thermal expansion coefficient and, similarly, $\beta_C = -(\partial\rho/\partial C)_{p,T}/\rho$ is the volumetric mass expansion coefficient relative to concentration C. The mixture density in the buoyancy term can thus be obtained from the reference value $\rho_L(T_L, C_L)$ as [26]

$$\rho = \rho_L[1 - \beta_T(T - T_L) - \beta_C(C - C_L)] \quad (1)$$

Usual situations correspond to positive β_T, the most frequent exception being the water between 0 °C and nearly 4.1 °C. On the other hand, usual situations can lead to either positive or negative β_C. If the overall fluid can be considered as a mixture of ideal gases, $\beta_T = 1/T_{abs}$ and $\beta_C = (M_2 - M_1)/[(M_2 - M_1)C + M_1]$, where M_1 is the molecular weight of the transported pollutant and M_2 is the molecular weight of the indifferent fluid. For the air–water vapor pair (the mixture considered in this work) at a temperature near 20 °C, β_T can assume values near $\beta_T = 0.0034$ and β_C can assume values between $\beta_C = 0.61$ (for $C = 0$) and $\beta_C = 0.38$ (for $C = 1$).

In energy conservation analysis, it is assumed that the thermal levels are small and similar enough so that the thermal radiation heat transfer between the walls is negligible, and the fluid is assumed to be radiatively non-participating. The energy terms due to viscous dissipation and change of temperature due to reversible deformation (work of pressure forces) are not considered. For the two-component mixture under analysis, there are not considered the energy terms of interdiffusional convection and diffusion thermo (Dufour effect) [27]. The only considered energy diffusion term is thus this due to Fourier conduction.

For the pollutant mass conservation, considered in this work through the ratio between the mass of pollutant to the total mass, $C = m_1/(m_1 + m_2)$, the only considered diffusional term is this due to Fick diffusion. The pressure diffusion, body force diffusion and thermal diffusion (Soret effect) terms are not considered [27]. If the mixture under analysis is the moist air, C is the specific humidity in a wet basis, which is related to the specific humidity in a dry basis, W, as $C = W/(1 + W)$.

The thermophysical properties of the involved media (two mixture components and the resulting mixture) are assumed to be constant, exception made to the density appearing in the buoyancy term, as explained above. In reality, the properties of the mixture that fills the cavity are dependent, between others, of the concentration level of the transported species and of the temperature level in each point of the enclosure.

It should be noted that the obtained results must be used with care, due to the real possibility of the non-considered condensation of the transported species. From psychrometry, noting that C is the specific humidity in a wet basis, for the air–water vapor pair one can obtain temperature and concentration levels that lead to relative humidities close to the unit (or even greater than 1), situation for which condensation of the transported species occur, as shown in [7].

2.3. Model equations

Taking the dimensionless variables

$$u_* = u/(\alpha/H); \quad v_* = v/(\alpha/H) \quad (2)$$

$$x_* = x/H; \quad y_* = y/H \tag{3}$$

$$T_* = (T - T_L)/(T_H - T_L);$$
$$C_* = (C - C_L)/(C_H - C_L) \tag{4}$$

$$p_* = (p + \rho_L g y)/[\rho_L(\alpha/H)^2] \tag{5}$$

where p_* is the dimensionless driving pressure, one obtains the following set of partial differential equations that govern the problem under analysis:

$$\frac{\partial u_*}{\partial x_*} + \frac{\partial v_*}{\partial y_*} = 0 \tag{6}$$

$$\frac{\partial}{\partial x_*}(u_* u_*) + \frac{\partial}{\partial y_*}(v_* u_*) = -\frac{\partial p_*}{\partial x_*} + Pr\left(\frac{\partial^2 u_*}{\partial x_*^2} + \frac{\partial^2 u_*}{\partial y_*^2}\right) \tag{7}$$

$$\frac{\partial}{\partial x_*}(u_* v_*) + \frac{\partial}{\partial y_*}(v_* v_*) = -\frac{\partial p_*}{\partial y_*} + Pr\left(\frac{\partial^2 v_*}{\partial x_*^2} + \frac{\partial^2 v_*}{\partial y_*^2}\right) + Ra_T Pr(T_* + NC_*) \tag{8}$$

$$\frac{\partial}{\partial x_*}(u_* T_*) + \frac{\partial}{\partial y_*}(v_* T_*) = \frac{\partial^2 T_*}{\partial x_*^2} + \frac{\partial^2 T_*}{\partial y_*^2} \tag{9}$$

$$\frac{\partial}{\partial x_*}(u_* C_*) + \frac{\partial}{\partial y_*}(v_* C_*) = \frac{1}{Le}\left(\frac{\partial^2 C_*}{\partial x_*^2} + \frac{\partial^2 C_*}{\partial y_*^2}\right) \tag{10}$$

Foregoing equations introduce the dimensionless parameters

$$Pr = \nu/\alpha; \quad Le = \alpha/D \tag{11}$$

$$Ra_T = \frac{g\beta_T(T_H - T_L)H^3}{\nu\alpha} \tag{12}$$

$$N = \frac{\beta_C(C_H - C_L)}{\beta_T(T_H - T_L)} \tag{13}$$

Another parameter that can be introduced is the Schmidt number, $Sc = \nu/D = PrLe$.

The Prandtl and thermal Rayleigh numbers are usual when analyzing the single natural convection heat transfer in enclosures. The N and Lewis parameters arise, in addition, when analyzing the double-diffusive natural convection problems. Parameter N is the buoyancy ratio, which is the ratio between the solute and thermal buoyancy forces. It can be either positive or negative, its sign depending of that of the ratio between the volumetric expansion coefficients β_T and β_C. When N is positive, the temperature and concentration buoyancy effects are combined, and they are opposite otherwise. When Eqs. (9) and (10) have the same boundary conditions, the T_* and C_* fields are coincident if $Le = 1$. It should be mentioned that a Rayleigh number referring to pollutant concentration analogous to Ra_T can be defined as $Ra_C = g\beta_C(C_H - C_L)H^3/\nu D$.

Multiple solutions or oscillatory solutions can be obtained for combined global heat and mass flows and negative values of parameter N [10,13,15], or for opposite global heat and mass flows and $0 < N < 1$ or N close to the unit. Considering, for example, the linear initial distributions $T_* = 1 - x_*$ and $C_* = x_*$, one obtains $T_* + NC_* = 1$, a result that is independent of x_*. All the points in the enclosure are under the same buoyancy effect, leading to a stagnant fluid situation. Any small disturbances, introduced by the initial conditions or by the numerical method of resolution, lead to different flow structures because they are generating differences in an initially expected uniform buoyancy field. These are situations not considered in the present work.

2.4. Boundary conditions

Over the walls of the enclosure it is

$$u_* = v_* = 0 \tag{14}$$

With such boundary conditions, it is assumed that the pollutant mass flow through the vertical walls is small enough in order to validate the use of zero normal velocity values at such walls.

Prescription of T_* and C_* over the vertical walls can lead to a situation of combined or opposite global heat and mass flows. Over the vertical walls it is thus prescribed that

$$T_*(0, y_*) = 1; \quad T_*[\cos\theta/(H/L), y_*] = 0 \tag{15}$$

$$C_*(0, y_*) = 1; \quad C_*[\cos\theta/(H/L), y_*] = 0 \quad \text{for combined heat and mass flows} \tag{16}$$

or

$$C_*(0, y_*) = 0; \quad C_*[\cos\theta/(H/L), y_*] = 1 \quad \text{for opposite heat and mass flows} \tag{17}$$

At the adiabatic and impermeable inclined walls of the enclosure it is

$$\frac{\partial T_*}{\partial n_*} = \frac{\partial C_*}{\partial n_*} = 0 \tag{18}$$

where n_* is the dimensionless normal to the inclined wall under consideration.

2.5. Heat and mass transfer parameters

The global heat and mass transfer rates can be evaluated once known the global Nusselt and Sherwood numbers, which are defined respectively as

$$Nu = \frac{\int_0^H -k\left(\frac{\partial T}{\partial x}\right)_{x=0} \mathrm{d}y}{k[(T_H - T_L)/L]H\cos\theta} = -\frac{1}{(H/L)\cos\theta}\int_0^1 \left(\frac{\partial T_*}{\partial x_*}\right)_{x_*=0} \mathrm{d}y_* \tag{19}$$

$$Sh = \frac{\int_0^H \rho D \left|\frac{\partial C}{\partial x}\right|_{x=0} \mathrm{d}y}{\rho D[(C_H - C_L)/L]H\cos\theta} = \frac{1}{(H/L)\cos\theta}\int_0^1 \left|\frac{\partial C_*}{\partial x_*}\right|_{x_*=0} \mathrm{d}y_* \quad (20)$$

As the inclined walls are impermeable and adiabatic, the derivatives $\partial T_*/\partial x_*$ and $\partial C_*/\partial x_*$ present in the global Nusselt and Sherwood numbers definitions can be taken at $x_* = 0$ or at $x_* = \cos\theta/(H/L)$. The modulus sign was introduced when defining the Sherwood number in order to define a positive value for this parameter, for both the situations of combined or opposite heat and mass flows. The reference situation for heat transfer, present in the denominator of Eq. (19), is the pure conduction situation through the stagnant fluid of thermal conductivity k, under the thermal gradient $(T_H - T_L)/L$, noting that the best value for the cross-section heat conduction area is $1 \times H\cos\theta$. The reference situation for mass transfer is obtained in a similar way.

2.6. Numerical modeling

The numerical method used in this work is a two-dimensional laminar version of the control-volume based finite element method described in [28]. A non-uniform structured 91×51 mesh, which expands from the walls towards the center of the enclosure in both directions, with an expansion factor of 1.05, was selected after some preliminary testes of asymptotic type.

3. Results and analysis

3.1. Values of the dimensionless parameters

The dimensionless parameters that govern the combined heat and mass transfer problem under analysis are six: Pr, Le, N, Ra_T, H/L, and θ. The highest temperature T_H and concentration C_H can be set at the same (left) vertical wall (combined global heat and mass flows) or on opposite vertical walls (opposite global heat and mass flows). Considering that the enclosure is filled with moist air, with a low concentration of water vapor, it can be taken $Pr = 0.7$, $Le = 0.8$, thus giving $Sc \approx 0.6$. For the moist air it is $(M_2 - M_1) > 0$, $\beta_C \geqslant 0$ and, consequently, $N \geqslant 0$, leading to situations with combined temperature and concentration buoyancy effects only. Parameters N, Ra_T, H/L and θ are changed in order to explore their influence on the structure of the resulting flow and on the heat and mass transfer performance of the enclosure. It is also made a short analysis of the situation corresponding to temperature and concentration boundary conditions leading to opposite global heat and mass flows.

3.2. Flow structure, temperature and concentration fields, and heat and mass transfer visualization

In order to illustrate the strong influence of the governing dimensionless parameters and boundary conditions over the flow structure (analyzed through the dimensionless streamlines), over the temperature and concentration fields (analyzed through their respective dimensionless contour plots), and over the heat and mass transfer taking place (analyzed through the dimensionless heatlines and masslines, respectively), a small set of results is presented and analyzed. The contour levels of the dimensionless heatlines and masslines do not match the numerical values of the global Nusselt and Sherwood numbers (these analyzed later, in Section 3.3), as expected [7,25,26]. This is due to the used definition for the Nusselt and Sherwood numbers, through Eqs. (19) and (20), and to the used reference values taken to obtain the dimensionless heatfunction and massfunction as $H_* = H/[k(T_H - T_L)]$ and $M_* = M/[\rho D(C_H - C_L)Le]$, respectively. The streamfunction was made dimensionless as $\psi_* = \psi/(\rho\alpha)$.

In Fig. 2 are presented the streamlines, isotherms and heatlines for the situation of a *square* $H/L = 1$ parallelogrammic enclosure, with $\theta = 30°$, $Ra_T = 10^5$ and no pollutant transfer ($N = 0$). These are figures with some resemblance with the well-known results for the differentially heated square enclosure [7,25], the inclination angle affecting considerably the variables' fields. It is also observed some symmetry on the streamlines and on the isotherms, which also exists on the differentially heated square enclosure [7,25].

Maintaining $Ra_T = 10^5$ and $N = 0$, but now for $H/L = 0.25$ and $\theta = 30°$ or $\theta = -30°$, considerable differences are observed, as presented in Fig. 3a (for $\theta = 30°$) and in Fig. 3b (for $\theta = -30°$). Comparing Figs. 2 and 3a, both for $\theta = 30°$ it is observed that when changing from $H/L = 1$ to $H/L = 0.25$ there is a strong change on the flow structure, which now spreads along the inclined enclosure's length. In the center of the enclosure, the streamlines are marked ellipses and not close to circles as for the *square* parallelogrammic enclosure with $H/L = 1$. The temperature field also changes considerably, with large regions of the central part of the enclosure subjected to nearly the same temperature level and intense temperature gradients near the vertical walls. In what concerns heat transfer, the observed changes on the streamlines are also reflected on the heatlines, being much more elongated, the heat flowing along the neighboring of the top inclined wall of the enclosure towards the right (cold) wall. Changing the inclination angle from $\theta = 30°$ to $\theta = -30°$ results in marked changes on all the process. The flow structure considerably changes, with a main clockwise vortex with two minor interior vertexes near the hot and cold vertical walls. The flow is much less intense than for

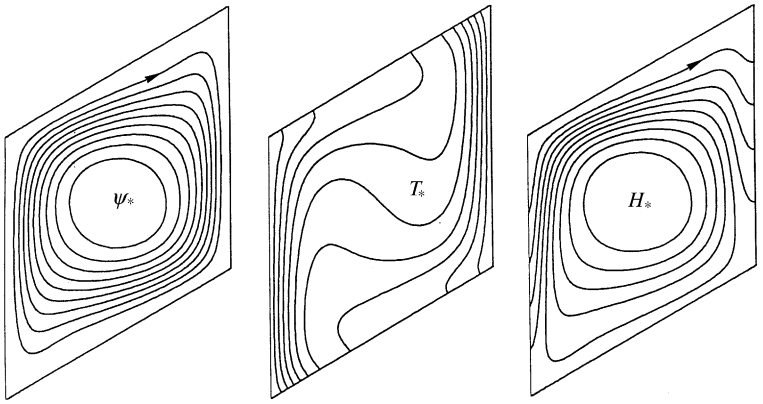

Fig. 2. Streamlines (left), isotherms (center) and heatlines (right), for the situation of non-pollutant transfer ($N = 0$), $\theta = 30°$, $H/L = 1$ and $Ra_T = 10^5$ ($\psi_{*,\min} = -14.43$, $\psi_{*,\max} = 0.00$, $\Delta\psi_* = 1.44$; $\Delta T_* = 0.10$; $H_{*,\min} = -4.96$, $H_{*,\max} = 4.53$, $\Delta H_* = 1.05$).

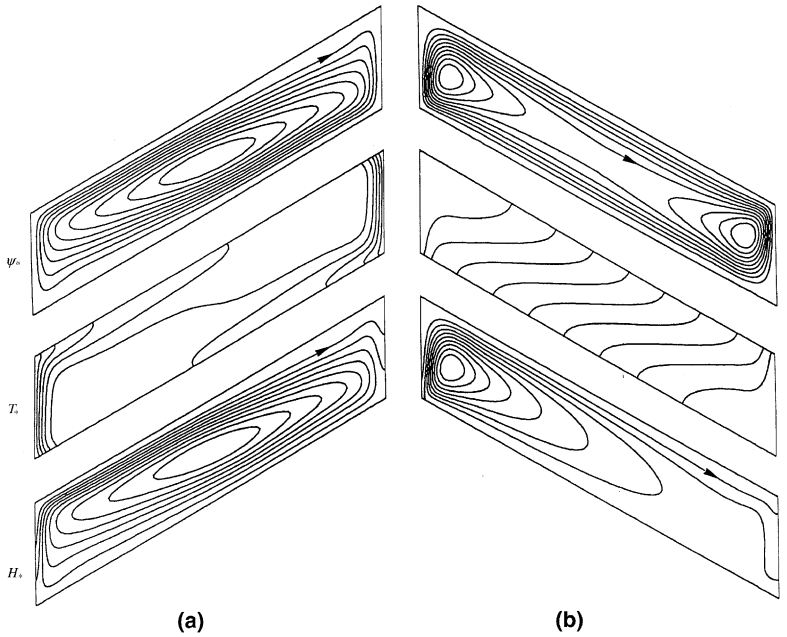

Fig. 3. Streamlines (top), isotherms (center) and heatlines (bottom), for the situation of non-pollutant transfer ($N = 0$), $H/L = 0.25$, $Ra_T = 10^5$ and (a) $\theta = 30°$ ($\psi_{*,\min} = -24.45$, $\psi_{*,\max} = 0.00$, $\Delta\psi_* = 2.44$; $\Delta T_* = 0.10$; $H_{*,\min} = -10.43$, $H_{*,\max} = 3.59$, $\Delta H_* = 1.40$); and (b) $\theta = -30°$ ($\psi_{*,\min} = -3.45$, $\psi_{*,\max} = 0.00$, $\Delta\psi_* = 0.34$; $\Delta T_* = 0.10$; $H_{*,\min} = -2.62$, $H_{*,\max} = 0.67$, $\Delta H_* = 0.33$).

$\theta = 30°$, as it can be obtained from the numeric values of the streamfunction. In what concerns the temperature field, it is observed a strong thermal stratification along the enclosure, the isotherms being nearly parallel one to each other, and nearly horizontal in the central region of the enclosure. This means that heat transfer through the enclosure occurs mainly by conduction. It is also observed that the temperature gradients near the vertical walls have considerably decreased, exception made to the lower-left and upper-right corners of the enclosure. In what concerns heat transfer, the heatlines show that heat is mainly extracted from the lower-left corner of the enclosure, and reaches the cold wall along a large portion of its length. The heat extracted from the remaining of the hot wall reaches the cold wall just near its upper-right corner. The main clockwise vortex observed on the flow field is also observed on the heatlines, but it remains near the hot left vertical wall of the enclosure. The heat transfer is much less intense (as expected from the analysis of the streamlines and of the temperature field), as it can be extracted from the numeric values of the heatfunction.

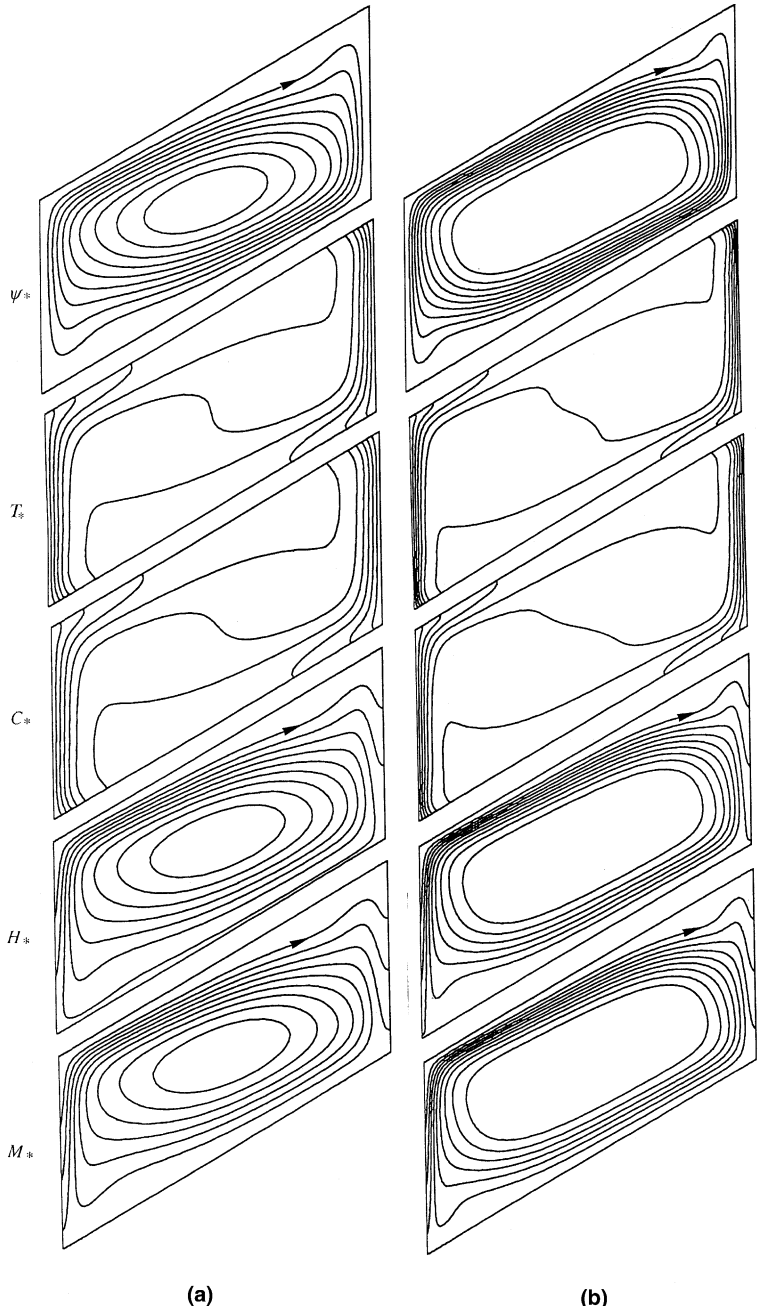

Fig. 4. Streamlines (top), isotherms (top-1), isoconcentrations (top-2), heatlines (top-3) and masslines (bottom), for combined global heat and mass flows, $H/L = 0.5$, $Ra_T = 10^5$, $\theta = 30°$ and (a) $N = 1$ ($\psi_{*,\min} = -28.33$, $\psi_{*,\max} = 0.00$, $\Delta\psi_* = 2.83$; $\Delta T_* = 0.10$; $\Delta C_* = 0.10$; $H_{*,\min} = -11.72$, $H_{*,\max} = 4.89$, $\Delta H_* = 1.66$; $M_{*,\min} = -11.44$, $M_{*,\max} = 5.46$, $\Delta M_* = 1.69$); and (b) $N = 10$ ($\psi_{*,\min} = -45.66$, $\psi_{*,\max} = 0.00$, $\Delta\psi_* = 4.57$; $\Delta T_* = 0.10$; $\Delta C_* = 0.10$; $H_{*,\min} = -18.81$, $H_{*,\max} = 8.17$, $\Delta H_* = 2.70$; $M_{*,\min} = -18.27$, $M_{*,\max} = 9.21$, $\Delta M_* = 2.75$).

The situation of combined global heat and mass flows, for $\theta = 30°$, $Ra_T = 10^5$ and $H/L = 0.5$ is presented in Fig. 4a for $N = 1$ and in Fig. 4b for $N = 10$. The changes from $N = 0$ to $N = 1$ are of minor importance on the results shown, the main changes from Fig. 3a to Fig. 4a being essentially due to the change from $H/L = 0.25$ to $H/L = 0.5$ and to the existence of pollutant mass transfer. Noticeable changes occur,

however, when N changes from $N = 1$ to $N = 10$. It should be noted that, in terms of the flow field, this corresponds nearly to a single natural convection heat transfer situation with $Ra_T = 10^6$. The flow is much more intense, and the temperature and concentration gradients have great values near the vertical walls, thus leading to considerably more intense heat and mass transfer for $N = 10$ than for $N = 1$. This can be numerically confirmed from the numeric values of the heatfunction and of the massfunction. As $Le = 0.8$, a value close to the unit, there are no marked differences on the temperature and concentration fields, as well as on the heatlines and masslines. Changing from $N = 1$ to $N = 10$ results in more intense flow field and more intense heat and mass transfer, which flows occur as closest to the top adiabatic and impermeable boundary of the enclosure as N increases.

Strong changes occur to the situation when the global heat and mass flows are opposite, and $N \gg 1$. Situations of $0 < N < 1$ or with N close to the unit are not explored, by the reasons explained before in Section 2.3. Results for opposite global heat and mass flows, $H/L = 0.5$, $\theta = 30°$, $Ra_T = 10^5$ and $N = 10$ are presented in Fig. 5. In what concerns flow structure, it comprises a major counter-clockwise vortex, with two minor interior counter-clockwise vertexes near the vertical walls. As the main contribution for buoyancy is that due to the concentration level, and the highest concentration is at the right vertical wall, the natural convection induced flow takes place through counter-clockwise vertexes. The main flow that reaches the left and right vertical walls takes place in thin regions adjacent to the upper and lower inclined walls of the enclosure. In what concerns the temperature and concentration fields, they present noticeable stratification at the center of the enclosure, the isotherms and the iso-concentration lines being markedly horizontal in a large portion of the central part of the enclosure. Intense temperature gradients are present near the upper-left and lower-right corners, associated with intense heat transfer rates in these regions. This fact can be observed from the heatlines, the heat flowing from the left vertical wall to the right vertical wall through a thin region adjacent to the lower inclined wall of the enclosure. The closed counter-clockwise loop on the heatlines is placed near the left vertical wall, of highest temperature level. This is a direct consequence of the main flow occurring in the form of counter-clockwise vertexes. The intense concentration gradients occur near the same upper-left and lower-right corners of the enclosure. However, the mass flow takes place, from the right vertical wall to the left vertical wall, through a thin region adjacent to the upper inclined wall of the enclosure, as clearly shown by the masslines. The closed counter-clockwise loop on the masslines is placed near the right vertical wall, of highest concentration level. The global heat and mass

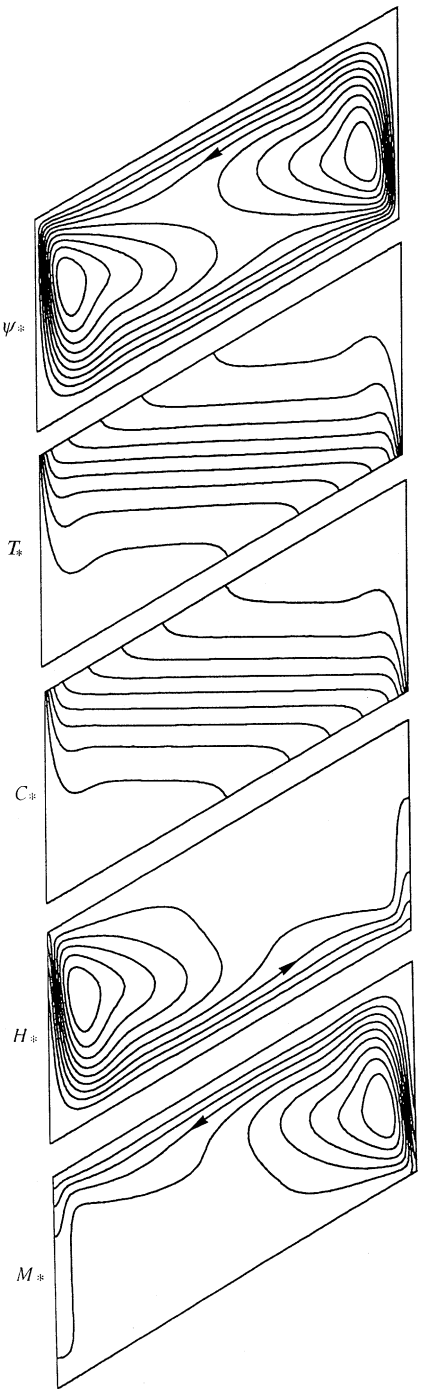

Fig. 5. Streamlines (top), isotherms (top-1), isoconcentrations (top-2), heatlines (top-3) and masslines (bottom), for opposite global heat and mass flows, $H/L = 0.5$, $Ra_T = 10^5$, $\theta = 30°$ and $N = 10$ ($\psi_{*,\min} = 0.00$, $\psi_{*,\max} = 7.66$, $\Delta\psi_* = 0.77$; $\Delta T_* = 0.10$; $\Delta C_* = 0.10$; $H_{*,\min} = 0.00$, $H_{*,\max} = 7.06$, $\Delta H_* = 0.71$; $M_{*,\min} = -2.92$, $M_{*,\max} = 4.35$, $\Delta M_* = 0.73$).

flows take place in opposite directions, under the marked influence of the advection associated with the mainly counter-clockwise fluid motion. Heat flows mainly through a thin region close to the lower inclined wall, and mass flows mainly through a thin region close to the upper inclined wall of the enclosure.

3.3. Global Nusselt and Sherwood numbers

The heat and mass transfer performance of the parallelogrammic enclosure is quantified through the global Nusselt and Sherwood numbers, as defined by Eqs. (19) and (20).

Analysis starts with the situation of no pollutant transfer ($N = 0$), being presented in Fig. 6a–c the global Nusselt number as function of the inclination angle θ and of the ratio H/L for values of $Ra_T = 10^3$, $Ra_T = 10^4$ and $Ra_T = 10^5$, respectively. For $Ra_T = 10^3$, whose results are presented in Fig. 6a, it is observed a similar behavior for $H/L = 0.1$ and for $H/L = 0.2$, with a nearly flat profile of Nusselt versus θ, the Nusselt number for $H/L = 0.2$ being always slightly higher than the Nusselt number for $H/L = 0.1$. For such cases, the global Nusselt number is only slightly greater than 1. When ratio H/L changes from 0.2 to 0.5, there is an increase on the Nusselt number, which is higher for low values of θ ($\theta \approx -60°$), intermediate values of θ ($\theta \approx 0°$), and high values of θ ($\theta \approx 60°$). For $H/L = 1$ there is a marked change on the behavior of the Nusselt number with the inclination angle θ, which considerably increases for low and high values of θ, and slightly decreases for intermediate values of θ.

It should be noted that the denominator $(H/L)\cos\theta$ in the definition of the Nusselt number (Eq. (19)) is a better description of the ratio $\dot{Q}_{\text{convection}}/\dot{Q}_{\text{conduction}}$ as H/L decreases, and that the so defined Nusselt number can increase two-times for low or high values of θ, due to the presence of $\cos\theta$ in the denominator of this equation. This is also valid for the Sherwood number.

As Ra_T increases from 10^3 to 10^4, significant changes occur in the Nusselt number dependence on θ, as it can be seen in Fig. 6b. It can be observed a general increase on the Nusselt number, relative to the situation of $Ra_T = 10^3$. However, the most noticeable change is given by the existence of marked maximum Nusselt numbers for $H/L = 0.1$, $H/L = 0.2$ and $H/L = 0.5$, the greatest value corresponding to $H/L = 0.2$. Such maximum values occur always for positive values of θ, nearly in the range 20–40°. Here it is markedly evident the thermal diode effect of the parallelogrammic enclosure, the Nusselt number for some positive values of θ being considerably higher than the Nusselt number for negative values $-\theta$. Selected positive values of θ allow heat transfer promoters and negative values of θ allow thermal insulation effect (for the specified temperature boundary conditions), by appropriate use of the parallelogrammic enclosure's shape. For $H/L = 1$, which presents a considerably flat profile of Nusselt versus θ, there is a general increase on the Nusselt number, relative to the situation of $Ra_T = 10^3$, which is more evident for intermediate values of θ.

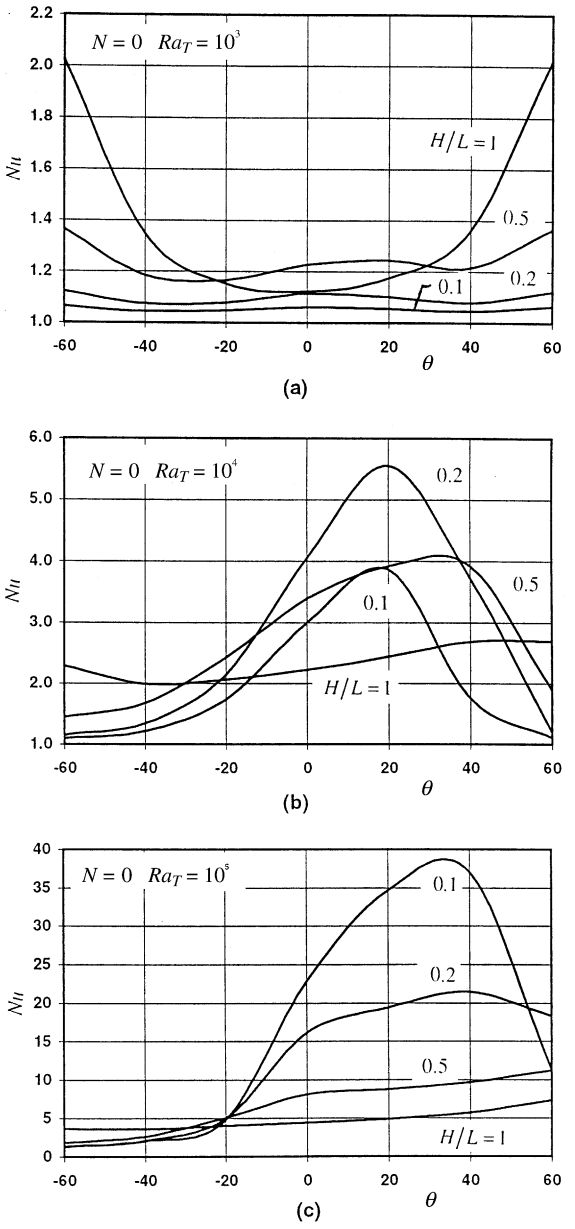

Fig. 6. Global Nusselt number versus inclination angle θ and ratio H/L for the situation of non-pollutant transfer ($N = 0$) and (a) $Ra_T = 10^3$; (b) $Ra_T = 10^4$; and (c) $Ra_T = 10^5$.

The situation corresponding to $Ra_T = 10^5$ is presented in Fig. 6b, where it is evident the small increase on the Nusselt number for lower values of θ and a marked increase of the Nusselt number for positive and

high values of θ and low values of the ratio H/L. There is evident the existence of maximum Nusselt numbers for $H/L = 0.1$ and $H/L = 0.2$, for θ near 40°, and monotonically increasing Nusselt numbers with θ for $H/L = 0.5$ and $H/L = 1$. The thermal diode effect is evident, and this effect increases as decreases the ratio H/L. For example, for $H/L = 0.1$, the ratio $[(Nu)_\theta/(Nu)_{-\theta}]_{\max}$ can reach values as high as nearly 25. It is also noticeable that the Nusselt number is almost constant and independent of θ for $\theta < -30°$.

The thermal diode effect can be explained in physical terms. For positive values of θ the hot fluid near the left vertical wall reaches the inclined upper wall which has a favorable inclination, allowing some tangentiality to the flow flowing up-right towards the cold wall. The same applies also for the descending cold fluid on the neighboring of the opposite vertical wall. The flow is intense and the thermal gradients near the vertical walls are high, thus resulting on high global heat transfer rates. For negative values of θ, the inclined wall has a non-favorable inclination, and the fluid tends to be trapped at the acute corners on the top of the hot wall and on the bottom of the cold wall of the enclosure, with a resulting marked thermal stratification. The flow is less intense and the thermal gradients are smaller near the vertical walls, giving rise to lower heat transfer rates. A similar explanation applies to the mass transfer diode effect, when pollutant transfer is present.

The situation corresponding to combined global heat and mass flows, for $N = 1$, is presented in Figs. 7a–c for values of Ra_T of 10^3, 10^4 and 10^5, respectively. In this case, as pollutant transfer occurs, there are also presented the figures corresponding to the global Sherwood number. In general terms, it can be observed that as $Le = 0.8 \approx 1$ there are no significant differences on behavior and on the numeric values of the Nusselt and Sherwood numbers. For $Ra_T = 10^3$ it is observed a noticeable increase on the Nusselt number for intermediate values of θ relative to the non-pollutant transfer situation in Fig. 6a. It is also observed the emergence of marked maximum values for the Nusselt and Sherwood numbers for $H/L = 0.1$, $H/L = 0.2$ and $H/L = 0.5$, which occur in the range $0° < \theta < 20°$. For $H/L = 1$, the Nusselt and Sherwood numbers maintain marked increases for low and high values of θ, the numeric values for θ being very close to the values for $-\theta$. For $Ra_T = 10^4$, in Fig. 7b, remains essentially the analysis made to Fig. 6b, now enlarged to include also the Sherwood number. The highest Nusselt number corresponds now to $H/L = 0.1$, and there is a general increase on the heat and mass transfer parameters due to the increase on the source term on the vertical momentum equation. When $Ra_T = 10^5$, in Fig. 7c, there is a marked maximum on the Nusselt and Sherwood numbers for $H/L = 0.1$. For $H/L = 0.2$ there is a strong increase on the Nusselt and Sherwood numbers for θ between −20° and 20°, and after 20° they monotonically increase with θ, without an identifiable maximum. For $H/L = 0.5$ and $H/L = 1$ it remains valid the analysis made for Fig. 6c, enlarged to include also the analysis of the Sherwood number behavior, with the expected increase on the transfer parameters due to the increase on the source term on the vertical momentum equation.

The situation corresponding to combined heat and mass flows and $N = 10$ is presented in Figs. 8a–c for $Ra_T = 10^3$, $Ra_T = 10^4$ and $Ra_T = 10^5$, respectively. The source term on the vertical momentum equation, $Ra_T Pr(T_* + NC_*)$, is nearly $10Ra_T Pr$ in the neighboring of the highest concentration wall. In this way, results in Fig. 7a have some similitude with the results in Fig. 6b. The same applies also to Figs. 7b and 6c. Fig. 7c represents the situation with the highest source term considered in the vertical momentum equation, with high numeric values for the Nusselt and Sherwood numbers, for high values of θ. As the source term on the vertical momentum equation increases so disappear the maximum values on the Nusselt and Sherwood numbers, which have an essentially increasing behavior with θ. In this case, the thermal diode effect for $H/L = 0.1$, evaluated as $[(Nu)_\theta/(Nu)_{-\theta}]_{\max}$, can reach values as high as nearly 50, which is remarkable. The same applies similarly to the mass transfer diode effect of the parallelogrammic enclosure. It is also noticeable that, for small values of the vertical momentum source term, the greatest heat and mass transfer parameters are obtained for the highest values of the ratio H/L, and high values of the source term lead to greater heat and mass transfer parameters for small H/L ratios. It should be mentioned that the heat and mass transfer diode effects increase as increases the vertical momentum source term, the transfer parameters for low values of θ remaining essentially unchanged.

Results for the opposite global heat and mass flows and $N = 10$ are presented in Figs. 9a–c, for $Ra_T = 10^3$, $Ra_T = 10^4$ and $Ra_T = 10^5$, respectively. In this case, the vertical momentum source term is conditioned essentially by the concentration field, which has its maximum at the right vertical wall of the enclosure. Thus, from the physical explanation given for the heat and mass transfer diode effects, the favorable inclination corresponds now to negative values of θ, and the non-favorable situation corresponds to positive values of θ. For $Ra_T = 10^3$, in Fig. 9a, there are marked maximum values on the Nusselt and Sherwood numbers for $H/L = 0.1$, $H/L = 0.2$ and $H/L = 0.5$, all for negative values of θ, the highest heat and mass transfer parameters occurring for $H/L = 0.2$. When Ra_T changes from 10^3 to 10^4, this in Fig. 9b, there is a considerable increase on the heat and mass transfer parameters for negative values of θ, with marked maximum values for $H/L = 0.1$ and $H/L = 0.2$. The region of the figure corresponding to high values of θ remains essentially

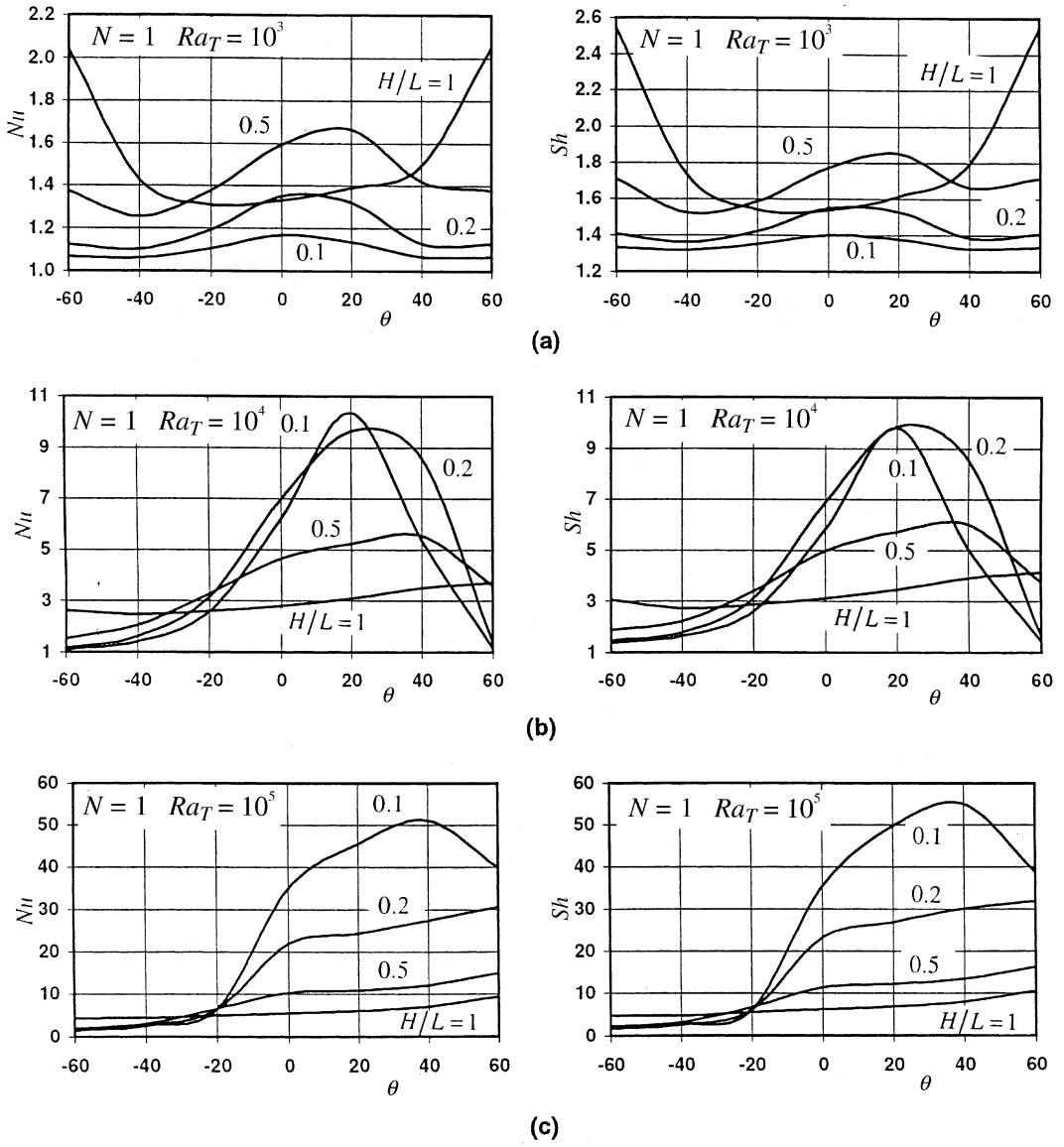

Fig. 7. Global Nusselt (left) and Sherwood (right) numbers versus inclination angle θ and ratio H/L for the situation of combined global heat and mass flows, $N = 1$ and (a) $Ra_T = 10^3$; (b) $Ra_T = 10^4$; and (c) $Ra_T = 10^5$.

unchanged. For $Ra_T = 10^5$, in Fig. 9c, it is noted a close similitude with Fig. 8c, but now with the highest heat and mass transfer parameters for the lower values of θ, and low heat and mass transfer parameters for high values of θ. In this case, there are also noticeable the heat and mass transfer diode effects. Their physical explanation remains the same as for combined global heat and mass flows, but now the highest transfer parameters occur for low values of θ and the minimum values on the heat and mass transfer parameters occur for high values of θ, as expected.

4. Conclusions

Parallelogrammic shape is very attractive as the basic shape to build, by assembly, more complete and complex structures that should present good heat and mass transfer performances. In particular, the parallelogrammic enclosures have strong potential to be used in the assembly of construction elements. As many of the construction elements, in the form of enclosures, are subject to heat and mass transfer and to the gravitational field, and are, in many situations, filled with moist air, present

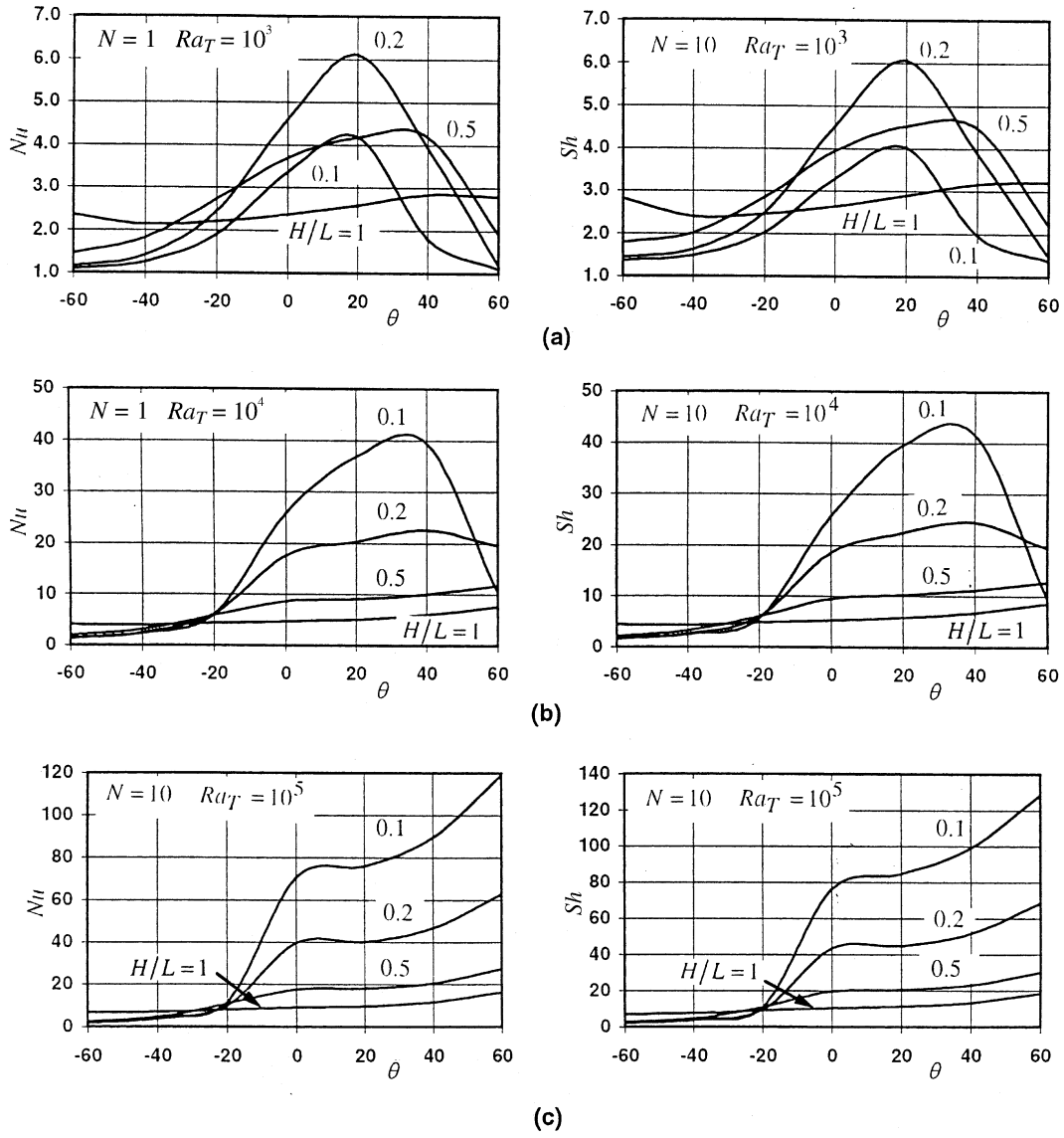

Fig. 8. Base legend as for Fig. 7, for $N = 10$.

study deals mainly with parallelogrammic enclosures filled with moist air. Even if the presented results refer to moist air only, the presented model is quite general. This work deals with double-diffusive natural convection in parallelogrammic enclosures, the non-solute transfer or the isothermal situations being simple particular cases.

In terms of the flow structure, temperature levels and concentration levels, strong changes occur in the parallelogrammic enclosure when changes are made on the Rayleigh number, the inclination angle and/or on the aspect ratio of the enclosure. Increasing the source term of the vertical momentum equation, by increasing the Rayleigh number (more severe boundary conditions) or by increasing the buoyancy ratio, always lead to increases on the heat and mass transfer performance of the enclosure. Such increases are, however, strongly dependent of the aspect ratio of the enclosure and of the inclination angle. Very different behaviors are also obtained for the combined or opposite global heat and mass flows that cross the parallelogrammic enclosure. This is of special interest because, in many practical situations, both situations can equally occur.

When dealing with construction elements filled with moist air, special attention needs to be given to the temperature and concentration levels at each point of the enclosure, as they can lead to condensation condi-

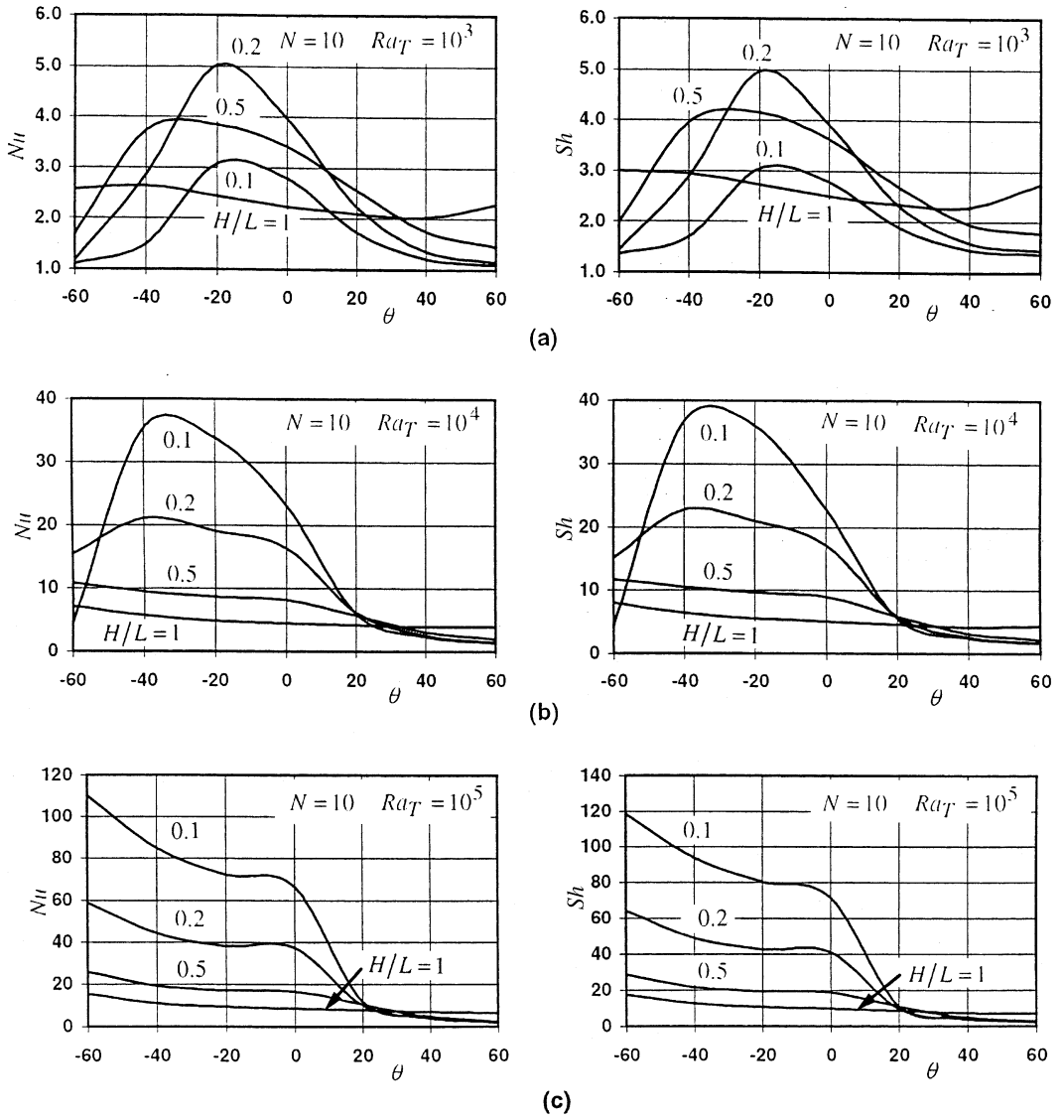

Fig. 9. Global Nusselt (left) and Sherwood (right) numbers versus inclination angle θ and ratio H/L for the situation of opposite global heat and mass flows, $N = 10$ and (a) $Ra_T = 10^3$; (b) $Ra_T = 10^4$; and (c) $Ra_T = 10^5$.

tions inside the enclosure. With careful control of the temperature and concentration levels, such (usually damaging) conditions can be avoided.

In what concerns the heat and mass transfer performance of the parallelogrammic enclosure, some main aspects should be mentioned. Selected combinations of the aspect ratio and of the inclination angle can lead to considerably high heat and mass flows through the enclosure, and some combinations of these parameters can even lead to the maximum allowable heat and mass transfer. This corresponds to the maximum transfer performance of the parallelogrammic enclosure, which is of crucial importance when it is to be used as a transfer promoter. Other selected inclination angles, of opposite sign from the foregoing ones, can lead to essentially unchanged poor transfer performance of the enclosure, thus giving rise to the notable transfer diode effect of the parallelogrammic enclosure: for a given aspect ratio, the ratio between the maximum of the transfer parameters to the respective minimum transfer parameters can be of some tenths. It is this marked directional transfer behavior of the parallelogrammic enclosure that, adequately conjugated with the temperature and concentration boundary conditions, gives to this shape so much

interest and so high potential to be used in components where heat and mass transfer processes are present.

References

[1] O.V. Trevisan, A. Bejan, Combined heat and mass transfer by natural convection in a vertical enclosure, ASME J. Heat Transfer 109 (1987) 104–112.

[2] H.K. Wee, R.B. Keey, M.J. Cunningham, Heat and moisture transfer by natural convection in a rectangular cavity, Int. J. Heat Mass Transfer 32 (9) (1989) 1765–1778.

[3] C. Béghein, F. Haghighat, F. Allard, Numerical study of double-diffusive natural convection in a square cavity, Int. J. Heat Mass Transfer 35 (4) (1992) 833–846.

[4] K. Kamakura, H. Ozoe, Experimental and numerical analysis of double diffusive natural convection heated and cooled from opposing vertical walls with an initial condition of a vertically linear concentration gradient, Int. J. Heat Mass Transfer 36 (8) (1993) 2125–2134.

[5] V.A.F. Costa, Convecção Natural Induzida por Diferenças de Temperatura e de Concentração numa Cavidade Quadrangular com Paredes Difusivas, in: Proc. of the III Congreso Iberoamericano de Ingeniería Mecánica (CIDIM'97) (CD edited), Habana, Cuba, 1997, work 2-275.

[6] V.A.F. Costa, Double diffusive natural convection in enclosures with heat and mass diffusive walls, in: G. De Vahl Davis, E. Leonardi (Eds.), Proc. of the International Symposium on Advances in Computational Heat Transfer (CHT'97), Begell House, New York, 1998, pp. 338–344.

[7] V.A.F. Costa, Double diffusive natural convection in a square enclosure with heat and mass diffusive walls, Int. J. Heat Mass Transfer 40 (17) (1997) 4061–4071.

[8] J. Tanny, B. Yakubov, The effect of layer depth on mixing in a double-diffusive two-layer system, Int. J. Heat Mass Transfer 45 (10) (2002) 2101–2105.

[9] F. Alavyoon, On natural convection in vertical porous enclosures due to prescribed fluxes of heat and mass at the vertical boundaries, Int. J. Heat Mass Transfer 36 (10) (1993) 2479–2498.

[10] M. Mamou, P. Vasseur, E. Bilgen, Multiple solutions for double-diffusive convection in a vertical porous enclosure, Int. J. Heat Mass Transfer 38 (10) (1995) 1787–1798.

[11] P. Nithiarasu, K.N. Seetharamu, T. Sundararajan, Double-diffusive natural convection in an enclosure filled with fluid-saturated porous medium: A generalized non-Darcy approach, Numer. Heat Transfer, Part A 30 (1996) 413–426.

[12] M. Karimi-Fard, M.C. Charrier-Mojtabi, K. Vafai, Non-Darcian effects on double-diffusive convection within a porous medium, Numer. Heat Transfer, Part A 31 (1997) 837–852.

[13] L. Kalla, M. Mamou, P. Vasseur, L. Robillard, Multiple solutions for double-diffusive convection in a shallow porous cavity with vertical fluxes of heat and mass, Int. J. Heat Mass Transfer 44 (23) (2001) 4493–4504.

[14] K. Benhadji, P. Vasseur, Double diffusive convection in a shallow porous cavity filled with a non-Newtonian fluid, Int. Commun. Heat Mass Transfer 28 (6) (2001) 763–772.

[15] Y. Masuda, M. Yoneya, T. Ikeshoji, S. Kimura, F. Alavyoon, T. Tsukada, M. Hozawa, Oscillatory double-diffusive convection in a porous enclosure due to opposing heat and mass fluxes on the vertical walls, Int. J. Heat Mass Transfer 45 (6) (2002) 1365–1369.

[16] A.J. Chamkha, Double-diffusive convection in a porous enclosure with cooperating temperature and concentration gradients and heat generation or absorption effects, Numer. Heat Transfer, Part A 41 (2002) 65–87.

[17] P. Bear, A. Khalili, Double-diffusive natural convection in an anisotropic porous cavity with opposing buoyancy forces: multi-solutions and oscillations, Int. J. Heat Mass Transfer 45 (15) (2002) 3205–3222.

[18] K. Khanafer, K. Vafai, Double-diffusive mixed convection in a lid-driven enclosure filled with a fluid-saturated porous medium, Numer. Heat Transfer, Part A 42 (2002) 465–486.

[19] K.C. Chung, L.M. Trefethen, Natural convection in a vertical stack of inclined parallelogrammic cavities, Int. J. Heat Mass Transfer 25 (2) (1982) 277–284.

[20] N. Seki, S. Fokosako, A. Yamaqushi, An experimental study of free convective heat transfer in a parallelogrammic enclosure, ASME J. Heat Transfer 105 (1983) 433–439.

[21] J.M. Hyun, B.S. Choi, Transient natural convection in a parallelogram-shaped enclosure, Int. J. Heat Fluid Flow 11 (2) (1990) 129–134.

[22] V.A.F. Costa, A.R. Figueiredo, L.A. Oliveira, Convecção Natural em Cavidades Paralelogrâmicas, in: Proceedings of the I Congreso Iberoamericano de Ingeniería Mecánica, vol. 2, E.T.S. Ingenieros Industriales, Madrid, 1993, pp. 255–260.

[23] M.-R. Zugari, J.-J. Vullierme, Étude numérique du transfert de chaleur dans une cavité de forme parallélogrammatique et inclinée, à parois pasives minces, Comptes Rendues à L'Academie des Sciences de Paris, Série II 319 (1994) 1157–1163.

[24] K.D. Aldridge, H. Yao, Flow features of natural convection in a parallelogrammic enclosure, Int. Commun. Heat Mass Transfer 28 (7) (2001) 923–931.

[25] V.A.F. Costa, Unification of the streamline, heatline and massline methods for the visualization of two-dimensional transport phenomena, Int. J. Heat Mass Transfer 42 (1) (1999) 27–33.

[26] A. Bejan, Convection Heat Transfer, second ed., Wiley, New York, 1995.

[27] E.R.G. Eckert, R.M. Drake Jr., Analysis of Heat and Mass Transfer, McGraw-Hill, New York, 1972.

[28] V.A.F. Costa, L.A. Oliveira, A.R. Figueiredo, A control volume based finite element method for three-dimensional incompressible turbulent fluid flow, heat transfer, and related phenomena, Int. J. Numer. Methods Fluids 21 (7) (1995) 591–613.